ELSEVIER

Contents lists available at ScienceDirect

## **Chemical Geology**

journal homepage: www.elsevier.com/locate/chemgeo





# Elemental composition of smectite minerals in continental rise sediments from the Amundsen Sea, West Antarctica, as a tool to identify detrital input from various sources throughout late Quaternary glacial-interglacial cycles

Young Kyu Park <sup>a</sup>, Claus-Dieter Hillenbrand <sup>b</sup>, Werner Ehrmann <sup>c</sup>, Hanbeom Park <sup>a</sup>, Julia S. Wellner <sup>d</sup>, Jennifer R. Horrocks <sup>e</sup>, Jinwook Kim <sup>a,\*</sup>

- <sup>a</sup> Department of Earth System Sciences, Yonsei University, Seoul, Republic of Korea
- <sup>b</sup> British Antarctic Survey, Cambridge, United Kingdom
- <sup>c</sup> Institute for Geophysics and Geology, University of Leipzig, Germany
- d Department of Earth and Atmospheric Sciences, University of Houston, Houston, TX, USA
- <sup>e</sup> Department of Geography, Durham University, Durham, United Kingdom

### ARTICLE INFO

Editor: Christian France-Lanord

Keywords:
Amundsen Sea
Elemental composition of smectite
Glacial-interglacial cycle
Sediment provenance
West Antarctic Ice Sheet

### ABSTRACT

Detrital smectite is a ubiquitous clay mineral in marine sediments and has a variable total Fe, Al, and Mg composition depending on the source, i.e., bedrock or unconsolidated sedimentary strata, the smectite is derived from. Analyses of elemental composition of smectite minerals in marine sediments can help to differentiate the smectite sources and, thus, sediment provenance, with potentially far-reaching paleo-environmental implications. In this study, we investigated the smectite compositions of modern-latest Holocene seafloor surface sediments deposited offshore from the Amundsen Sea drainage sector, where the West Antarctic Ice Sheet is currently unstable and losing mass due to ocean-forced melting, to detect and understand the variabilities of their elemental composition and geographical distribution. The smectite composition in continental rise sediments was compared to that of potential source areas on the Amundsen Sea continental shelf and in the sub-Antarctic South Pacific basin. Furthermore, we analyzed the smectite composition of sediments in continental rise cores deposited during the last glacial and last interglacial periods to reconstruct source variations over glacialinterglacial cycles. In particular, high contents of Al-Fe-rich smectite indicate that the glacial sediments had been supplied from the coastal region around Pine Island Bay by the cross-shelf advance of the West Antarctic Ice Sheet during the last glacial period. This clearly contrasts with the smectite minerals in rise sediments deposited during the present and the last interglacial periods that are composed of two distinct smectite types (Mg-rich and Al-rich, respectively), indicating their supply from multiple sources. During interglacials, Mg-rich smectite is probably transported by Circumpolar Deep Water from the sub-Antarctic South Pacific basin to the continental rise, while Al-rich smectite is supplied as part of ice rafted debris and by marine currents from the coasts around the Amundsen Sea embayment. Our research demonstrates that analysis of the elemental composition of smectite minerals on the Amundsen Sea continental margin provides a valuable tool to trace variations in sources for detrital sediment components and their pathways throughout glacial-interglacial cycles.

### 1. Introduction

The West Antarctic Ice Sheet (WAIS) is a largely marine-based ice sheet, and has undergone significant thinning and retreat in its Amundsen Sea drainage sector over the last four decades (e.g. Rignot et al., 2019; Smith et al., 2020). It has been suggested that current deglaciation of this sector may culminate in future WAIS collapse in

response to continued global warming, which could contribute up to ca. 3–4 m to global sea-level rise (DeConto and Pollard, 2016; Vaughan, 2008). The current mass loss in the Amundsen Sea sector is associated with the upwelling of relatively warm Circumpolar Deep Water (CDW) that intrudes to the inner shelf, causing increased basal melting of ice shelves there and reducing the buttressing effect of these ice shelves for grounded glaciers feeding into them (e.g. Jacobs et al., 2012; Jenkins

E-mail address: jinwook@yonsei.ac.kr (J. Kim).

<sup>\*</sup> Corresponding author.

et al., 2016; Pritchard et al., 2012). These findings that were largely obtained by remote sensing over the last few decades suggest potential WAIS instability, which has been corroborated by ice-sheet model runs (e.g. DeConto and Pollard, 2016). However, to fully comprehend the dynamical behavior of the WAIS, the model simulations need to be complemented with and validated by the long-term ice-sheet record archived in continental margin sediments deposited offshore from the WAIS. Particularly, sedimentary sequences from the Antarctic continental rise can provide valuable high resolution records of ice sheet dynamics and paleo-environmental changes (e.g. Escutia et al., 2009; Hillenbrand and Ehrmann, 2005) because in contrast to sediment records from the shelf and slope erosion by glacial-overriding or reworking by gravitational processes usually do not occur there. Detrital components of marine sediments on the continental rise supplied from the nearby continental shelf or surrounding ocean areas, can be used to reconstruct environmental changes over a wide region. For example, the terrigenous detritus can give clues about delivery of glacigenic debris by the ice sheet, hemipelagic sediment input by the eastward flowing Antarctic Circumpolar Current (ACC, Fig. 1), and/or supply of suspended particles by regional bottom currents (Hillenbrand et al., 2021; Lucchi et al., 2002; Lucchi and Rebesco, 2007).

An effective strategy for reconstructing past ice sheet dynamics and transport of glacigenic detritus is to investigate sediment provenance using the mineralogical and geochemical characteristics of marine sediments deposited at the periphery of the ice sheet (Cook et al., 2013; Hillenbrand et al., 2003; Licht and Hemming, 2017; Williams et al.,

2010; Wilson et al., 2018). For example, depositional processes and transport pathways of terrigenous detritus at present and in the past have been inferred from the spatial and temporal variations in the relative proportions of clay minerals on the continental rise and in the deep sea and their comparison with those of potential source rocks and shelf sediments in nearby coastal areas (Biscaye, 1965; Hillenbrand and Ehrmann, 2001; Hillenbrand et al., 2009a; Hillenbrand et al., 2009b; Hillenbrand et al., 2010; Jung et al., 2019; Pandarinath, 2009; Park et al., 2019; Petschick et al., 1996). Along the West Antarctic continental margin the sources of clay mineral assemblages deposited on the rise have been traced to their potential sources on the Antarctic continent by mapping of distinct clay mineral provinces on the shelf, i.e., a "smectite province" around the South Shetland Islands (northwestern Antarctic Peninsula), a "chlorite province" along the western Antarctic Peninsula coast, an "illite province" offshore from Ellsworth Land, and a "kaolinite province" on the Amundsen Sea shelf (Ehrmann et al., 2011; Hillenbrand and Ehrmann, 2001; Hillenbrand et al., 2003). However, in seafloor surface sediments from the Amundsen Sea continental rise, unusually high smectite contents had been observed that were too high to be explained by smectite supply from nearby shelf sediments only (Ehrmann et al., 2011). Several possibilities were proposed to explain these relatively high smectite contents on the rise: 1) supply from the volcanic Peter I. Island by a westward flowing bottom current; 2) eastward supply in bottom water originating from the Ross Sea region by the ACC; or 3) southward supply of smectite-rich clay from the sub-Antarctic South Pacific basin by a deep-water current (Ehrmann et al., 2011;

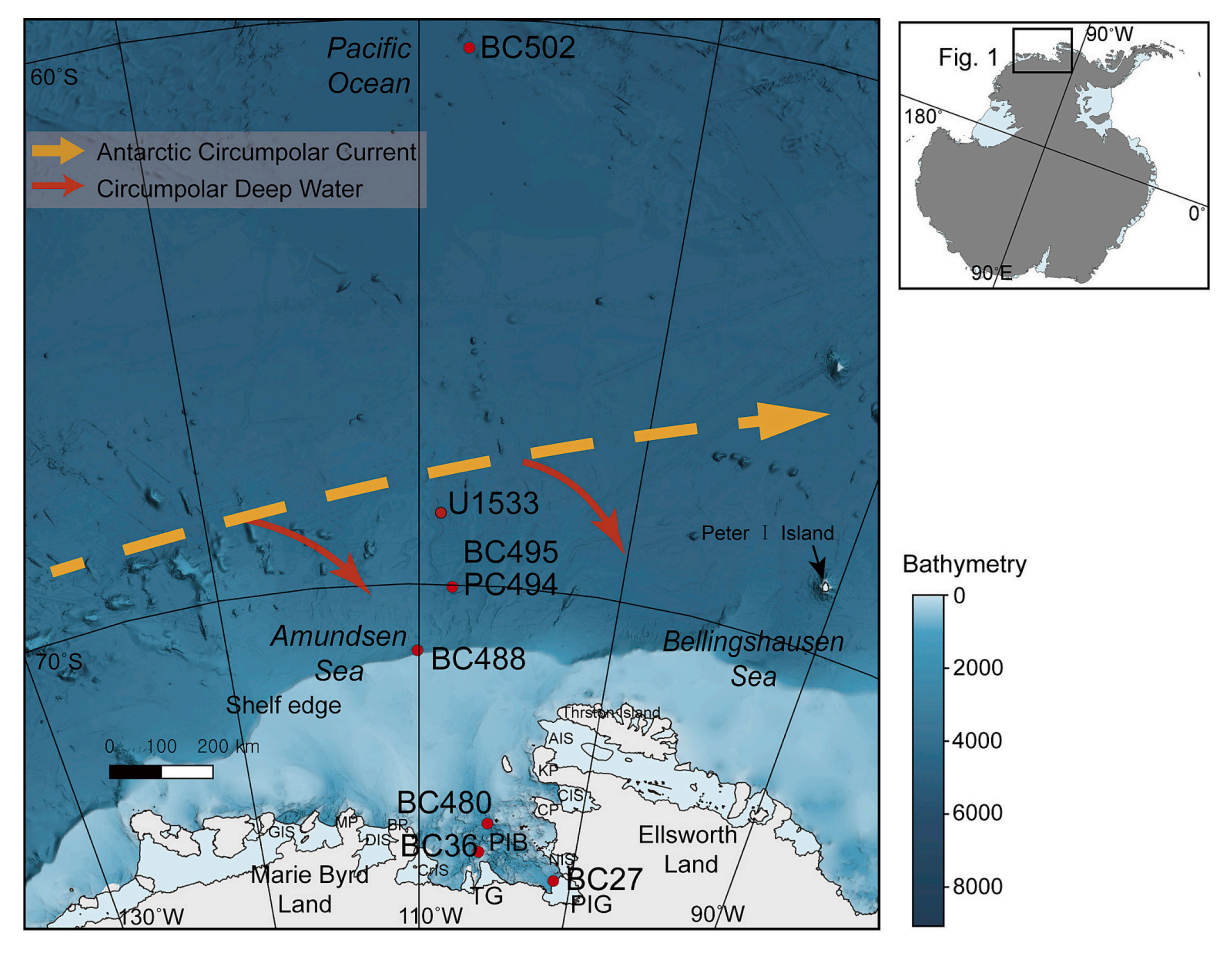


Fig. 1. Location of core samples, BC27 (Pine Island Glacier front), BC36 (Thwaites Glacier), BC480, and BC488 on the Amundsen Sea shelf and slope, BC495/PC494 and U1533 on the Amundsen Sea continental rise and sample BC502 in the sub-Antarctic South Pacific basin. Schematic ocean circulation modified from Totten et al. (2017). Bathymetry obtained from Dorschel et al. (2022). AIS = Abbot Ice Shelf, BP = Bear Peninsula, CIS = Cosgrove Ice Shelf, CP = Canisteo Peninsula, CrIS = Crosson Ice Shelf, DIS = Dotson Ice Shelf, GIS = Getz Ice Shelf, KP = King Peninsula, MP = Martin Peninsula, NIS = Northern Ice Shelf, PIB = Pine Island Bay, PIG = Pine Island Glacier, TG = Thwaites Glacier.

Hillenbrand et al., 2003). However, none of these hypotheses could be confirmed or refuted by analyzing the clay mineral assemblages alone, even though such studies demonstrated that the smectite contents were also increased in pre-Holocene interglacial sediments on the eastern Amundsen Sea continental rise (Hillenbrand et al., 2009b; Horrocks, 2018).

Thus, smectite minerals in Amundsen Sea sediments may play a critical role for reconstructing provenance and paleo-environmental changes. The term "smectite" is often referred as a group name to swelling 2:1 layered clay-sized phyllosilicates with water molecules and various cations in the interlayer (Weaver and Pollard, 1973). For example, depending on variation in the octahedral cations, nontronite (Fe-rich), saponite (Mg-rich), and montmorillonite-beidellite (Al-rich) can be distinguished (Velde, 1995; Weaver and Pollard, 1973). Smectites in deep-sea sediments can be of detrital origin or originate from authigenic processes (Chamley, 1994; Deconinck and Chamley, 1995; McKinley et al., 1999). Detrital smectites can be derived from the continent as a product of chemical weathering of volcanic or igneous rocks under warm, semi-arid climate conditions (Chamley, 1989; Righi and Meunier, 1995), or as a product of physical weathering and glacial reworking of hydrothermally altered volcanic bedrock and tephra under (sub-)polar conditions (Jeong et al., 2004). Smectites can also be derived from sediments or metamorphic rocks (Drief and Nieto, 2000). The smectite composition (dioctahedral or trioctahedral smectite) usually depends on the mineral or chemical composition of the weathered source bedrock and sedimentary strata (McKinley et al., 1999). Authigenic smectites can form by the hydrothermal alteration of volcanic glass or volcanic rocks (Chamley, 1989). These authigenic smectites are typically Fe-rich (nontronite) or Mg-rich (saponite) (Hillier, 1995). Distinguishing the different types of smectite may therefore allow to determine transport pathways of sedimentary particles from continental and oceanic sources. Recently, analysis of smectite minerals in late Quaternary marine sediments from the southern Drake Passage and Bellingshausen Sea has been used to reconstruct transport pathways of sedimentary detritus from its West Antarctic sources (Park et al., 2019).

In this study, the elemental compositions of smectite minerals in seafloor surface sediments from the Amundsen Sea continental rise were analyzed by transmission electron microscopy (TEM) and compared with the compositions of smectite minerals in seafloor surface sediments from potential source areas, i.e., the Amundsen Sea continental shelf and the sub-Antarctic South Pacific basin. In addition, sources of smectites in continental rise sediments deposited during the last glacial period and the last interglacial period were investigated to reconstruct glacial-interglacial changes in sediment transport. The results suggest that elemental composition of smectites can be utilized as a new, powerful tool to trace sediment provenance, and improve our understanding of provenance changes in the paleo-record and its relation to past variations in WAIS extent and drainage.

### 2. Materials and methods

### 2.1. Samples

Six seafloor surface sediment samples (0–1 cmbsf depth of BC27 and BC36; 0–3 cmbsf depth of BC480, BC488, BC495 and BC502 [cmbsf: centimeters below seafloor]) recovered with box corers from the Amundsen Sea, including three shelf, one slope, one rise and one abyssal sample, were analyzed for this study. Core BC480 comes from Pine Island Bay, BC488 from the upper continental slope, BC495 from the continental rise, BC502 from the sub-Antarctic South Pacific basin, BC27 from the Pine Island Glacier front, and BC36 from the Thwaites Glacier front (Fig. 1, Table 1). Our strategy for sample site selection took into account the following two considerations: First, Pine Island Glacier (PIG) and Thwaites Glacier (TG) are by far the largest glacial systems draining ice – and, thus, presumably glacigenic debris – into the Amundsen Sea. Second, previously published results of clay mineral

Table 1 Sediment core information in this area. BC = box core; PC = piston core.

Core	Sample depth (cm)	Age	Location	Sediment description
BC480	0–3	Modern- late Holocene	Amundsen Sea, inner continental shelf (Pine Island Bay)	Brownish mud
BC488	0–3	Modern- late Holocene	Amundsen Sea, upper continental slope	Brownish foraminiferal mud
PC494	199–202	MIS 2-4	Amundsen Sea, drift crest on continental rise	Laminated to stratified terrigenous mud
PC494	496–498	MIS 5e	Amundsen Sea, drift crest on continental rise	Foraminifera bearing mud
BC495	0–3	Modern- late Holocene	Amundsen Sea, drift crest on continental rise (very close to site PC494)	Brownish foraminiferal mud
BC502	0–3	Modern- late Holocene	Sub-Antarctic South Pacific basin	Brownish diatomaceous ooze
BC27	0–1	Modern- late Holocene	Amundsen Sea, inner continental shelf (Pine Island Glacier front)	Olive-brown mud with traces of diatoms
BC36	0–1	Modern- late Holocene	Amundsen Sea, inner continental shelf (Thwaites Glacier front)	Olive-brown sandy mud with traces of diatoms
U1533A 1H-1	54–55	MIS 5e	Amundsen Sea, drift flank on continental rise	Brown bioturbated diatomaceous ooze

investigations as well as neodymium and strontium isotope analyses on the fine-grained fractions of seafloor surface sediments in the region had revealed that the provenance fingerprints of detritus supplied by PIG and TG are progressively modified along the detritus transport pathway northwards across the shelf by admixture of detritus delivered by ice draining the eastern coastline of the Amundsen Sea embayment and glaciers draining into the Amundsen Sea to the west of TG (Ehrmann et al., 2011; Simões Pereira et al., 2018; Simões Pereira et al., 2020).

Seafloor surface sediments at sites BC488 and BC495 are composed of brownish foraminiferal mud, at site BC480 of brownish mud, and at site BC502 of diatomaceous ooze. Based on sedimentation rates derived from existing age models for various cores from the continental shelf and rise of the eastern Amundsen Sea and the sub-Antarctic South Pacific basin (Clark et al., 2024; Esper and Gersonde, 2014; Hillenbrand et al., 2009b; Hillenbrand et al., 2013; Horrocks, 2018; Kirshner et al., 2012), the seafloor surface sediments have a modern to late Holocene age.

In addition, two down-core samples from piston core PC494, which was – together with nearby box core BC495 – recovered from a sediment drift on the continental rise, were analyzed for this study. A glacial sample was obtained from laminated to stratified terrigenous mud at a core depth of 199–202 cmbsf deposited during Marine Isotope Stage (MIS) 2–4 (14–57 ka) and an interglacial sample was obtained from foraminifera bearing-mud at 496–498 cmbsf depth deposited during MIS 5e (116–130 ka) (Horrocks, 2018). For comparison, another sample from sediments deposited during MIS 5e was analyzed from International Ocean Discovery Program (IODP) Expedition 379 Site U1533 (Fig. 1), which had been drilled on the same sediment drift (Gohl et al., 2021). The sample was taken from 54 to 55 cm depth in core section U1533A 1H-1, which corresponds to a subseafloor depth of 2.50 m.

#### 2.2. Sample preparation

Sample preparation for X-ray diffraction (XRD) analysis followed the methods described by Jackson (1969). The sediment samples were treated with hydrogen peroxide (30%  $\rm H_2O_2$ , 9.79 M) to disperse the particles by removing the organic matter. In addition, the sediment samples were treated with 1 N NaOAc (pH 5) to remove carbonate (Jackson, 1969). The clay fraction  $<2~\mu{\rm m}$  was then collected through centrifugation at 1000 rpm for 2 min. Air-dried clay samples, prepared by the filter–peel method using a 0.45- $\mu{\rm m}$  membrane filter paper, were placed on a slide glass for the diffractometer measurements (Moore and Reynolds Jr, 1989), and then the mounts were solvated overnight with ethylene glycol in a desiccator to measure an ethylene-glycolated clay sample.

Sediment samples were also impregnated with LR White resin followed by the structural water exchange procedure (Kim et al., 1995) to measure the petrophysical properties of smectite using transmission electron microscopy (TEM). This method allows to prevent the collapse of the smectite layer to 10 Å identical to mica when subjected to the high-energy electron beam during TEM operation, and thus to distinguish smectite layers by measuring layer spacing (Kim et al., 1995). The impregnated samples were cut into 120-nm thick sections using a diamond knife ultramicrotome (ULTRACUT UCT, Leica, installed at Eulji University, Seongnam, Korea) and then placed on a holey carbon TEM grid (Kim et al., 1995; Yang et al., 2016).

### 2.3. X-ray diffractometry

The XRD profiles of the air-dried and glycolated clay samples were recorded in the range  $2^{\circ}$ – $40^{\circ}$  20 and  $2^{\circ}$ – $30^{\circ}$  20, respectively, with a scanning speed of 1.5°/min at a step size of 0.02° using a Rigaku MiniFlex II diffractometer at Yonsei University, Seoul (Korea), with a CuKα radiation source at 30 kV and 15 mA. The receiving and divergence slit sizes were 0.3 mm and 1.25°, respectively. The Crystallographica Search-Match program (version 2.0.3.1) was used to identify the major clay minerals and semi-quantitative analysis of clay minerals were performed by comparing the basal reflections for the glycolated and airdried XRD profiles (method in the Appendix A). For the glycolated sample, clay minerals were identified by 17 Å peak for smectite, 10 Å peak for mica, and 7 Å peak for chlorite and kaolinite. Kaolinite and chlorite were differentiated by resolving the (002) kaolinite peak and (004) chlorite peak at 3.57 and 3.54 Å, respectively (Biscaye, 1964; Ehrmann et al., 2011). Semi-quantification of R0 mica/smectite mixed layer in the glycolated samples was confirmed by Sybilla method (Drits and Sakharov, 1976; McCarty et al., 2009). R1 mica/smectite mixed layer was confirmed by the appearance of peaks at 9.84° and 15.74° 20 (Kim et al., 2019; Park et al., 2024).

### 2.4. Transmission Electron Microscopy (TEM)

A JEOL JEM-F200 transmission electron microscope fitted with an energy-dispersive X-ray spectrometer (EDS) at Yonsei University was operated at a voltage of 200 kV to acquire the physico-chemical properties of smectite. K-factors for EDS analysis can be obtained by the transformation of intensity ratio to concentrations of real standards (Cliff and Lorimer, 1975). Theoretically calculated standard can generate error of chemical quantification compared to the directly determined in the used equipment with standard materials (Conconi et al., 2023). However, the difference between calculated factor and real factor of major elements in smectite are not dramatics (Conconi et al., 2023), not greatly affecting to the final quality of the structural formula of smectite. In addition, all smectite analyses were performed with the same equipment, so the same errors affected all analyses, and comparisons are not affected by these errors. Hundreds of bright-field lattice fringe images with corresponding selected-area electron diffraction (SAED) patterns and EDS for smectite clay minerals were recorded; they

were analyzed using the DigitalMicrograph TM software (Version 3.22. 1461. 0, Gatan Inc., Pleasanton, CA, USA).

# 2.4.1. Determining elemental composition of smectite and visualization in a ternary diagram

The quantification of structural composition of smectite was calculated based on 10 oxygen atoms and 2 hydroxyl groups (Christidis et al., 2023; Marshall, 1935). In total, we analyzed ~240 smectite packets from all sediment samples (at least 10 packets per sample). Because of limitation of TEM-EDS quantification, the distribution of Al between tetrahedral and octahedral position and possibility of interlayer Mg could be affected by the intrinsic errors. Therefore, the overall proportions of the Al-Mg-Fe instead of the octahedral cation in smectite minerals from each sediment samples are compared. The composition ratio of total Al-Mg-Fe of individual smectite minerals from each surface sediment sample characterizing a potential source area (i.e., samples BC480, BC488, BC27, BC36 and BC502) are summarily shown as a compositional field for each sample in the ternary diagram, whereas the Al-Mg-Fe ratios of individual smectite minerals from the sediment samples of cores PC494, BC495 and U1533 are plotted as individual data points in the same ternary diagram (Appendix A; Table A.2-10 and Appendix B). Furthermore, the similarity between the total Al, Mg, and Fe compositions of smectites from each sediment sample was evaluated using the Kolmogorov-Smirnov (K-S) method (Stuart and Ord, 1999). The K-S statistical test is a nonparametric test expressing the cumulative distributions of data which are compared both visually and by cumulative frequencies. The maximum absolute difference between the two cumulative distribution functions (D-statistic) determines the similarity, with a smaller D-statistic value indicating stronger similarity (Appendix A; Table A.11).

### 3. Results

### 3.1. Clay mineral composition

Major components of the clay fraction <2 µm of the sediment samples (BC495, PC494, BC480, BC488, BC502, BC27, and BC36) are the clay minerals smectite (Sme, 17 Å, glycolated), Mica (Mca, 10 Å), chlorite (Chl, 14 and 7 Å) and kaolinite (Kln, 7 Å), which were identified in XRD profiles for the air-dried and ethylene-glycolated samples (Fig. 2). Non-clay minerals, such as quartz (Qz), plagioclase (Pl), and pyroxene (Px) were also identified in all clay samples. Kaolinite and chlorite were differentiated by resolving the (002) kaolinite peak and (004) chlorite peak at 3.57 and 3.54 Å, respectively (Fig. 2). The proportion of clay minerals from continental shelf (BC480, BC27, and BC36) sediment are high mica contents (28-67%), while sediment (BC502) from South Pacific Basin reveals a relatively high content of smectite (49%) and low content of kaolinite (5%). Furthermore, it is noticeable that clay mineral contents in BC495 (smectite (22%), mica (45%) and kaolinite (14%)) and in MIS 5 in PC494 (smectite (31%), mica (43%) and kaolinite (9%)) are clearly contrast with those in MIS 2-4 in PC494 (smectite (16%), mica (54%), and kaolinite (19%)) (Appendix A; Table A.1). The appearance of R1 mica/smectite mixed layers is not measured (XRD peak at 9.84° and 15.74° 20) for the samples (Fig. 2), except BC36 showing minor content of R0 mica/smectite mixed layer (~6 wt%) confirmed by Sybilla method (Appendix A; Table A.1) resulting in the relatively intense smectite peak (17 Å) after glycolation.

### 3.2. Results of Transmission Electron Microscopy (TEM) analysis

# 3.2.1. Identification of smectite minerals and semi-quantification of their composition by energy-dispersive X-ray spectrometry (EDS)

Representative TEM micrographs of clay packets show layer spacings ranging from 1.1 to 1.3 nm and layer terminations on the lattice fringe images that correspond to a diffuse  $d_{001}=1.09$ –1.17 nm of SAED

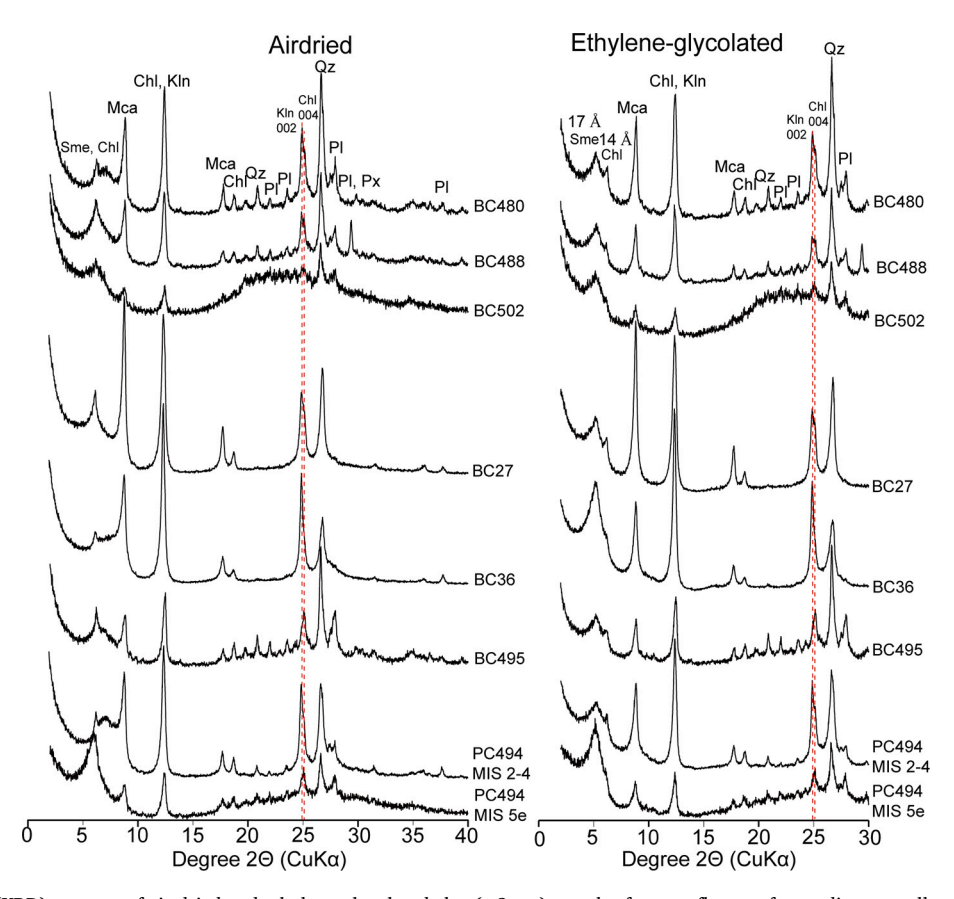


Fig. 2. X-ray diffraction (XRD) patterns of air-dried and ethylene-glycolated clay ( $<2 \mu m$ ) samples from seafloor surface sediments collected at sites BC480, BC488, BC495, BC502, BC27 and BC36, and from MIS 2–4 (last glacial period) and MIS 5e (last interglacial) sediments from site PC494 on the continental rise. There is a clear separation of chlorite (14 Å) and smectite (17 Å) after glycolation. Kaolinite was identified by a separation of kaolinite (002) peak at 24.9°2 $\theta$  and chlorite (004) peak at 25.1–25.2°2 $\theta$  (red dotted line). Sme: smectite, Chl: chlorite, Kln: kaolinite, Mca: mica, Pl: plagioclase, Qz: quartz, and Px: pyroxene. (For interpretation of the references to colour in this figure legend, the reader is referred to the web version of this article.)

patterns (insets in Fig. 3a), typical for smectite. The aforementioned inset diffuse SAED patterns indicate that the smectite layers have a turbostratically disordered structure due to the variations in elemental composition, layer periodicity, and layer terminations. Structural elemental compositions of the smectites revealed by TEM-EDS (Fig. 3b) show a lower Al/Si ratio ( $\sim$ 0.4), K ( $\sim$ 0.2) and variations in octahedral cations (Fe, Al, Mg) (Table 2, and Appendix A; Table A.2–10). Representative EDS spectra of the smectite minerals from cores BC495, PC494 (MIS 5e) and BC502 show a higher intensity of Mg compared to smectite minerals in the other sediment samples. The average structural formula of smectites from all surface sediment samples are summarized in Table 3.

### 3.2.2. Al-Fe-Mg compositions of smectites

The compositional Al-Fe-Mg fields defined by the composition of the smectite minerals from potential modern sediment sources, such as PIG (BC27), TG (BC36), Pine Island Bay (BC480), the eastern Amundsen Sea embayment slope (BC488), and the sub-Antarctic South Pacific basin (BC502), are given in Appendix A. Tables A.2, A.3, A.7, A.8, A.9 and visualized in the ternary diagram of Fig. 4, where also the smectite compositions of modern-late Holocene (BC495) as well as last glacial and last interglacial (both PC494) sediment samples from the continental rise are plotted. The smectites from the continental shelf and slope (BC27, BC36, BC480 and BC488) have on average high Al contents (58%; full range 23–91%), intermediate Fe contents (29%; full range 7–64%) and low Mg contents (13%; full range 2–27%) (Appendix B). The smectites from the sub-Antarctic South Pacific basin (BC502) reveal on average intermediate Mg (31%; full range 16–55%), Fe (39%; full range 17–55%) and Al contents (30%; full range 8–67%). Smectites in

modern–late Holocene sediments from continental rise site BC495 are on average characterized by high Al contents (52%; full range 23–90%) and intermediate Fe (28%; full range 3–48%) and Mg contents (20%; full range 7–47%). This composition differs from that of smectite minerals deposited at nearby rise site PC494 during MIS 2–4, which have on average comparable Fe contents (25%; full range 14–39%), but higher Al (62%; full range 46–76%), and lower Mg contents (13%; full range 10–21%). The smectite minerals in the MIS 5e sediments of continental rise cores PC494 and U1533 have on average intermediate Al (45%; full range 17–72%), Fe (38%; full range 12–59%) and Mg contents (20%; full range 11–36%) (Appendix B). In general, the Al, Mg and Fe contents in smectites of interglacial sediments from the Amundsen Sea continental rise show a relatively large compositional variability.

### 3.3. K—S tests of smectite compositions

The Al-Mg-Fe compositions of smectites in the interglacial and glacial sediments from rise sites PC494 and BC495 were statistically compared with those of smectites from potential source areas on the Amundsen Sea shelf and in the sub-Antarctic South Pacific basin using cumulative distribution functions (Fig. 5) and D-statistics (Appendix A; Table A.11). The cumulative distributions of Al, Mg, and Fe in smectites from the glacial sample from core PC494 are visually similar to those of smectites in modern-late Holocene sediments from the Amundsen Sea continental shelf and slope. This similarity is also evident from the D-statistics of Al (0.3), Mg (0.3) and Fe (0.3). The cumulative distributions of Al, Fe and Mg composition in smectites from the interglacial samples at rise sites PC494 and U1533 (MIS 5e) as well as BC495 (modern-late Holocene) have intermediate values between those of smectites on the

Y.K. Park et al. Chemical Geology 657 (2024) 122116

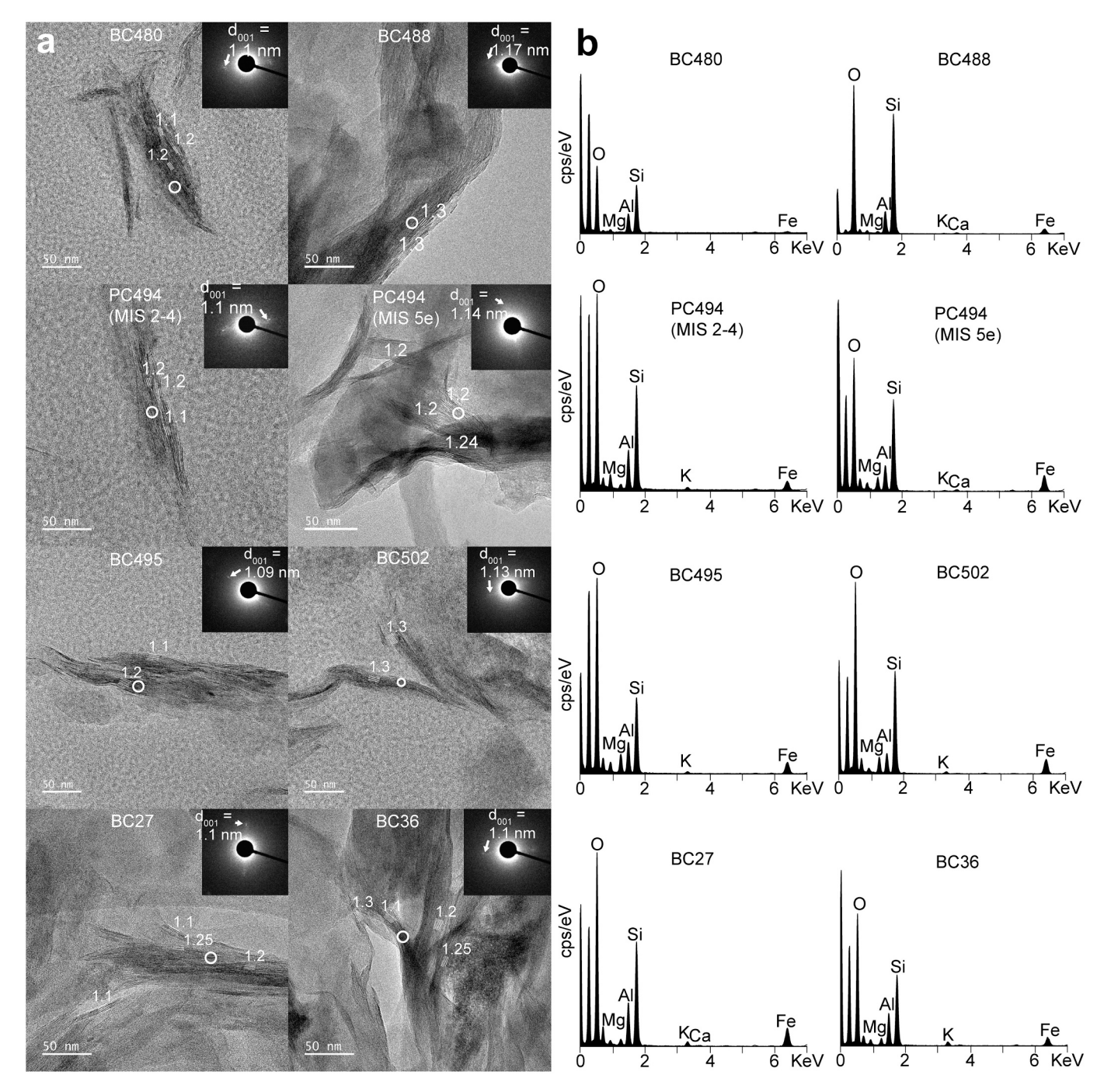


Fig. 3. Representative TEM micrographs of lattice fringes in smectites and corresponding selected-area electron diffraction (SAED) pattern ( $d_{001} = 1.09-1.17$  nm) from (a) BC480, BC488, PC494 (MIS 2–4), PC494 (MIS 5e), BC495, BC502, BC27, and BC36. (b) Representative EDS spectra of smectite in each sample showing compositional variations reflecting supply from different sources (white circle).

continental shelf and slope and in the sub-Antarctic South Pacific basin. Similarity of elemental compositions between interglacial smectites from rise sites BC495 [Al (0.64), Mg (0.47) and Fe (0.60)] and PC494 and U1533 (MIS 5e) [Al (0.48), Mg (0.56) and Fe (0.27)] and modernlate Holocene smectites from site BC502 was calculated in D-statistics (Appendix A; Table A.11).

### 4. Discussion

## 4.1. Geographical variability in elemental composition of smectite

The clay mineral assemblages in core BC495 and PC494 (MIS 5e) in

continental rise exhibit significantly higher smectite contents than MIS 2–4 in PC494 (Appendix A; Table A.1). It is necessary to distinguish various types of smectite likely to be transported from multi-provenance (Park et al., 2019) on the Amundsen Sea continental rise. The elemental compositions of smectites from the potential source areas on the Amundsen Sea shelf and slope (BC27, BC36, BC480, BC488) and the sub-Antarctic South Pacific basin (BC502) define two groups: 1) Al–rich smectites (neatly dioctahedral smectite) with intermediate Fe contents in samples from the former area and 2) additional presence of Mg-rich smectites (minor component of trioctahedral smectite and/or montmo-rillonite component) in the sample from the latter area (Fig. 4, Table 2 and Appendix B). Smectites in the sediments samples in this study are in

Table 2
Compositional range of elemental composition of smectites from each investigated sample (calculated with O = 10 and OH = 2) obtained by TEM-EDS (Appendix A; Table A. 2–10).

Sample	Sample Tetrahedral sheet		Octahedral sheet				Interlayer		Number of smectites		
	Si	Al(4)	Al(6)	Mg	Fe	Ti	Mn	K	Ca	Na	analyzed
BC495	3.23-3.99	0.01-0.77	0.39-1.81	0.14-1.1	0.07-1.25	0-0.13	0-0.05	0.01-0.36	0.01-0.13	0-0.2	53
PC494 (MIS 2–4)	3.39–3.94	0.06-0.61	0.83-1.55	0.21-0.62	0.3-0.9	0-0.05	0-0.03	0.01-0.47	0-0.03	0	10
PC494 (MIS 5e)	3.12-3.99	0.01-0.88	0.07-1.4	0.23-0.73	0.39–1.7	0-0.12	0-0.25	0-0.34	0.06-0.39	0-0.25	63
BC480	3.22-3.99	0.01 - 0.78	0.54 - 1.82	0.04-0.5	0.15-1.27	0-0.06	0	0.01 - 0.37	0.01-0.05	0	10
BC488	3.44-3.93	0.07 - 0.56	0.29 - 1.5	0.1 - 0.65	0.34 - 1.48	0-0.07	0	0-0.37	0.04 - 0.25	0	21
BC27	2.99-3.91	0.09 - 1.01	0.18 - 1.43	0.19 - 0.82	0.36 - 1.81	0-0.1	0-0.03	0.04-0.44	0.01-0.04	0	18
BC36	3.3-3.98	0.02-0.7	0.54-1.5	0.13 - 0.67	0.35 - 1.37	0-0.07	0-0.06	0-0.2	0-0.08	0 - 0.23	36
BC502	3.45-3.98	0.02 - 0.55	0.12 - 1.33	0.33 - 1.39	0.37 - 1.4	0.01-0.09	0-0.03	0-0.3	0.01 - 0.04	0	21
U1533	3.22-3.94	0.06-0.78	0.12-1.4	0.26 - 0.89	0.29 - 1.5	0-0.08	0-0.05	0-0.29	0-0.06	0-0.25	17

Table 3 Average structural formula of smectites from each investigated sample (calculated with  $\rm O=10$  and  $\rm OH=2$ ) obtained by TEM-EDS.

Sample	Average structural formula
BC495	$\begin{array}{l} (\text{Ca}_{0.04}\text{K}_{0.13}\text{Na}_{0.04})(\text{Al}_{0.97}\text{Mg}_{0.5}\text{Fe}_{0.68}\text{Ti}_{0.02}\text{Mn}_{0.01})(\text{Si}_{3.72}\text{Al}_{0.28}) \\ \text{O}_{10}(\text{OH})_2 \end{array}$
PC494 (MIS 2–4)	$(Ca_{0.01}K_{0.2})(Al_{1.17}Mg_{0.33}Fe_{0.61}Ti_{0.01}Mn_{0.01})(Si_{3.71}Al_{0.29})O_{10}(OH)_2$
PC494 (MIS 5e)	$(Ca_{0.14}K_{0.08}Na_{0.03})(Al_{0.74}Mg_{0.47}Fe_{0.86}Ti_{0.03}Mn_{0.03})(Si_{3.69}Al_{0.31})$ $O_{10}(OH)_2$
BC480	$(Ca_{0.02}K_{0.15})(Al_{1.12}Mg_{0.31}Fe_{0.68}Ti_{0.02})(Si_{3.71}Al_{0.29})O_{10}(OH)_2$
BC488	$\begin{array}{l} (\text{Ca}_{0.12}\text{K}_{0.1}\text{Na}_{0.02})(\text{Al}_{1.01}\text{Mg}_{0.32}\text{Fe}_{0.74}\text{Ti}_{0.01}\text{Mn}_{0.01})(\text{Si}_{3.72}\text{Al}_{0.28}) \\ \text{O}_{10}(\text{OH})_2 \end{array}$
BC27	$(Ca_{0.02}K_{0.18})(Al_{1.02}Mg_{0.39}Fe_{0.76}Ti_{0.02}Mn_{0.01})(Si_{3.53}Al_{0.47})$ $O_{10}(OH)_2$
BC36	$\begin{array}{l} (\text{Ca}_{0.03}\text{K}_{0.08}^{-}\text{Na}_{0.08})(\text{Al}_{1.12}\text{Mg}_{0.3}\text{Fe}_{0.71}\text{Ti}_{0.01}\text{Mn}_{0.01})(\text{Si}_{3.67}\text{Al}_{0.33}) \\ \text{O}_{10}(\text{OH})_2 \end{array}$
BC502	$(Ca_{0.02}K_{0.09})(Al_{0.55}Mg_{0.75}Fe_{0.92}Ti_{0.02}Mn_{0.01})(Si_{3.83}Al_{0.17})$ $O_{10}(OH)_2$
U1533	$\begin{array}{l} (Ca_{0.02}K_{0.08}Na_{0.12})(Al_{0.8}Mg_{0.52}Fe_{0.86}Ti_{0.02}Mn_{0.01})(Si_{3.64}Al_{0.36}) \\ O_{10}(OH)_2 \end{array}$

general dioctahedral smectite, however sums of octahedral cations higher than 2 (Appendix A; Table A.2–10), likely due to the interlayer Mg or mixing with minor content of trioctahedral smectites. Hence, when sum of the octahedral cation is too high and the interlayer charge is too low as noted interlayer Mg must be present in Table A.2–10 in Appendix A (Elert et al., 2018; García-Romero et al., 2021; Sánchez-Roa et al., 2018).

Al-Fe rich smectites in sample BC27 recovered in front of PIG are probably supplied with detritus derived from pre-Oligocene sediments that contain weathering products of altered Jurassic granites and Paleozoic-Mesozoic granitoids underlying the PIG drainage basin (Simões Pereira et al., 2018; Simões Pereira et al., 2020). These acidic and intermediate igneous rocks are mainly composed of quartz, plagioclase and alkali feldspar. Of that, plagioclase and alkali feldspar can produce dioctahedral smectites as weathering products (Aoudjit et al., 1995). The presence of pre-Oligocene sedimentary strata is indicated by the relatively high content of kaolinite, which is a typical weathering product of (sub-)tropical climate conditions, both in sample BC27 and in other sediment samples close to the PIG grounding line (Ehrmann et al., 2011; Simões Pereira et al., 2020). Some additional relatively Fe-rich smectite may come from weathering products of Ferich minerals (i.e. biotite and pyroxene), which are typical components of mafic-rich basaltic rocks or volcaniclastics (Chang et al., 1986; Hillier, 1995). Basaltic rocks of Miocene to recent age are widespread in the hinterland of the Amundsen Sea embayment (e.g. LeMasurier, 2013; Simões Pereira et al., 2018), with the presence of hyaloclastic deposits at volcanic centers documenting that some eruptions occurred in contact with ice (e.g. LeMasurier, 2002), which may have produced smectite.

Abundant Al-rich and Fe-rich smectites in sample BC36 recovered in

front of TG are likely supplied with detritus originating from subglacial mafic volcanic rocks (de Vries et al., 2018) and biotite-bearing granitoids, as also suggested by Sr and Nd isotope data (Simões Pereira et al., 2020). Again, these smectites are highly likely to be eroded from sedimentary strata containing detritus derived from these igneous rocks (Drief and Nieto, 2000), because the kaolinite contents in sample BC36 and other samples taken in front of TG are even higher than in samples close to PIG (Ehrmann et al., 2011; Simões Pereira et al., 2020). Minor contents of R0 mica/smectite mixed layer supported detrital sediment could be also derived from diagenetic sediments (Nieto et al., 1996). Even though there are hardly any outcrops within the TG and PIG catchments, which makes it difficult to accurately interpret the geological sources for the smectites, our findings together with previously published data (Ehrmann et al., 2011; Simões Pereira et al., 2018; Simões Pereira et al., 2020) point to recycling and mixing of detritus during subglacial erosion and transport.

Sample BC480 from Pine Island Bay indicates supply of some additional Al-rich smectite minerals, which may reflect delivery of detritus derived from the east coast of Pine Island Bay (Canisteo Peninsula) and/or eroded by glaciers feeding into the Crosson Ice Shelf directly to the east of TG (Simões Pereira et al., 2020), and from sedimentary strata, such as the Cretaceous to early Neogene sediments cropping out at/near the seabed on the southern Amundsen Sea embayment shelf (Gohl et al., 2017; Klages et al., 2020; Nieto et al., 1996).

Notably, the Mg contents of smectites in the shelf samples never exceed 27%, whereas the smectites in sample BC502 from the sub-Antarctic South Pacific basin have Mg contents up to 55%. These Mgrich smectites probably result from the submarine alteration of volcanic glass or oceanic crust basalt, including ferro-magnesian minerals in hydrothermal environments (García-Romero et al., 2005; Hillier, 1995; McKinley et al., 1999; Mcmurtry and Yeh, 1981). Such processes have been reported from the sub-Antarctic South Pacific basin (Hollister and Worstell, 1976).

Smectite minerals in the Amundsen Sea continental rise samples PC494 and BC495 are, as in other Neogene and Quaternary Antarctic continental rise sediments (e.g. Escutia et al., 2009; Hillenbrand and Ehrmann, 2005), probably mainly of detrital origin but may also include authigenic smectites formed in the sub-Antarctic Pacific basin. High K contents in interlayer of smectite (higher than Ca), also supported that those smectite, are mainly detrital smectites in marine environments (Drief and Nieto, 2000). Smectites in the glacial sediments at site PC494 have high Al- and low Mg-contents, comparable to smectites in the modern-late Holocene sediments from the Amundsen Sea continental shelf (Fig. 4). In contrast, the smectite assemblages in the interglacial rise sediments (MIS 1 [0-14 ka] in BC495 and MIS 5e in PC494 and U1533) include, besides Al and Fe enriched smectite minerals, additionally Mg enriched smectites (Fig. 4 and Table 2). In this respect, the smectites deposited on the Amundsen Sea continental rise during interglacial periods, especially the smectites in core BC495, show some

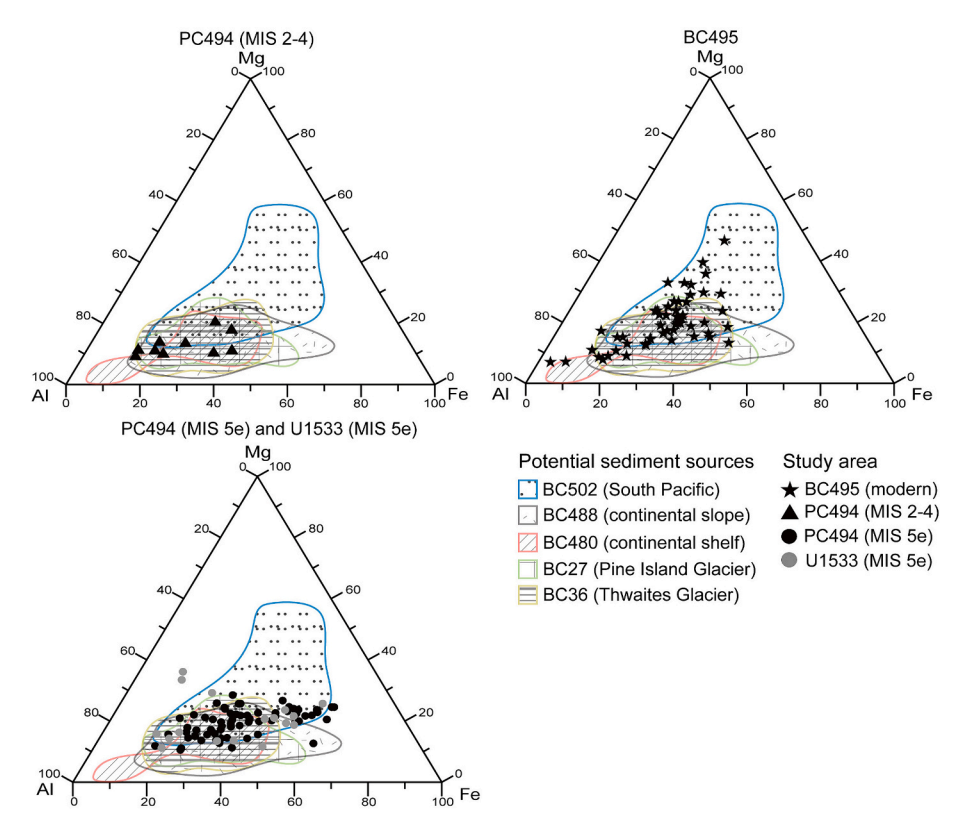


Fig. 4. Total Al-Fe-Mg compositions of the smectite minerals for samples BC495, PC494 and U1533 (Amundsen Sea continental rise) plotted in ternary diagrams (stars: BC495, triangles: PC494 MIS 2–4, black circles: PC494 MIS 5e, gray circles: U1533 MIS 5e). Compositional fields shown for potential sediment source samples encircle all Al-Fe-Mg compositions of individual smectite minerals analyzed for each source sample: BC502 (sub-Antarctic South Pacific basin), BC480 (Pine Island Bay), BC488 (Amundsen Sea continental slope), BC27 (Pine Island Glacier front), and BC36 (Thwaites Glacier front).

similarity to smectites from site BC502 in the sub-Antarctic South Pacific basin (Fig. 4). In addition, the most frequent of smectites in continental shelf are predominantly beidellites, but some smectites in BC495 and BC502 recognized by Si near 4 atoms per formula unit and high Mg contents are closely corresponding to montmorillonite (or intermediate cases). (Weaver and Pollard, 1973). This finding suggests that during interglacials minor quantities of trioctahedral Mg-rich smectites and/or montmorillonite components (Mg-rich) are advected southwards from the sub-Antarctic South Pacific Basin towards the Amundsen Sea continental margin by bottom and deep waters, such as CDW. The cumulative distribution functions (Fig. 5) and D-statistics (Appendix A; Table A.11) confirm the similarity of smectite elemental compositions in the interglacial continental rise samples with those in BC502.

However, the Mg contents in smectites from the MIS 5e samples of cores PC494 and U1533 are generally lower (<36%) than in smectites from the nearby surface sediment sample BC495 (<47%), and the MIS 5e smectites also contain less Al (<72%) but more Fe (<59%) than the smectites in the surface sediment sample (Al <90%, Fe <48%; Appendix B). These differences in Al, Mg and Fe contents between late-Holocene and MIS 5e smectites from the Amundsen Sea continental rise could be due to different environmental conditions between the modern and the last interglacial. For example, less Al-rich smectite might have been supplied to the deep Amundsen Sea from the Antarctic continent during MIS 5e, when the WAIS is assumed to have been much more retreated than today (e.g., DeConto and Pollard, 2016; Dutton et al., 2015; Lau et al., in press). Alternatively, bottom water advection to the Amundsen Sea continental rise during MIS 5e could have been different from MIS 1. All studied rise sites are today located within the eastward flowing ACC (Gohl et al., 2021; Horrocks, 2018). Grain-size proxy data from a sediment core in Drake Passage have shown that ACC flow speed was not only consistently higher during interglacials than during glacials throughout the last 1.3 Myr, but also that ACC current speed was higher

during MIS 5e than during MIS 1 (Toyos et al., 2020). This may indicate that during the last interglacial period more fine-grained detrital particles originating from the Ross Sea sector, including smectites with a different Al-Mg-Fe composition, were advected eastward to the Amundsen Sea continental rise than during the present interglacial.

# 4.2. Sediment transport to the Amundsen Sea continental rise throughout a glacial-interglacial cycle

Based on the possible sources of smectite in the Amundsen Sea sector of West Antarctica and the sub-Antarctic South Pacific basin identified in this study and previously reported temporal changes in clay mineral assemblages on the Amundsen Sea continental rise (Hillenbrand et al., 2002; Hillenbrand et al., 2009b; Horrocks, 2018), the following transport and depositional model for glacial-interglacial cycles is suggested (Fig. 6).

During a glacial period, the grounding line of the WAIS advanced across the Amundsen Sea shelf to or at least close to the shelf edge (cf. Gohl et al., 2013; Larter et al., 2014). This ice advance was focused in paleo-ice streams that emanated from the mouths of major modern ice streams, such as PIG and TG (Larter et al., 2014), from where the potential source samples for this study were selected. Moreover, annual sea ice cover over the continental slope and rise lasted much longer during glacial periods than during interglacial periods and was possibly even perennial during glacial maxima (Bostock et al., 2013; Konfirst et al., 2012). During the glacial maxima the merged Pine Island-Thwaites paleo-ice stream accumulated large volumes of eroded glacigenic debris at the shelf break. This material was subsequently transported down the continental slope by gravitational processes, such as slumps and debris flows, and further down to the continental rise by turbidity currents, with bottom currents redistributing the fine-grained particles and accumulating them as sediment drifts (Dowdeswell et al., 2006; Y.K. Park et al. Chemical Geology 657 (2024) 122116

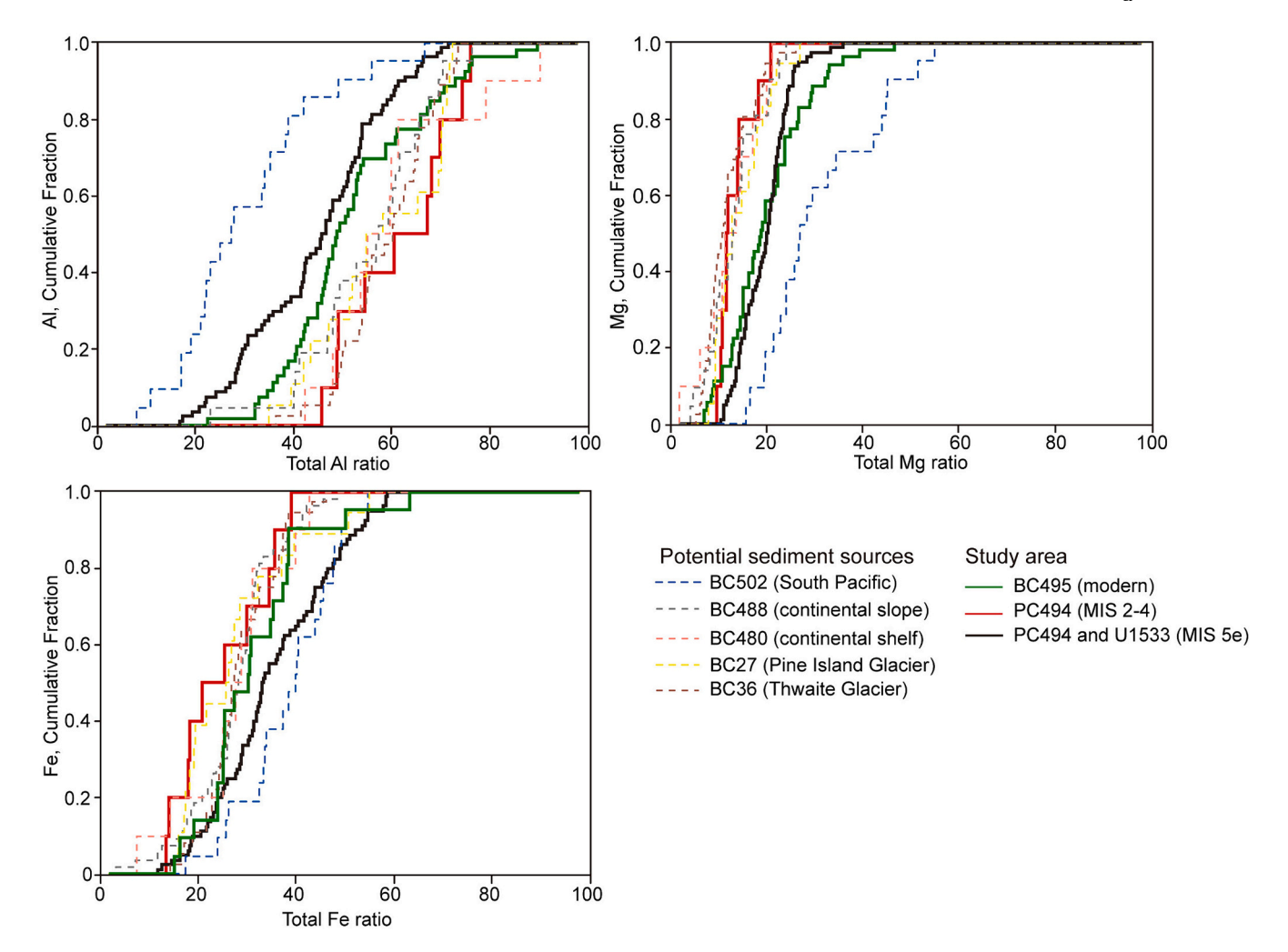


Fig. 5. Kolmogorov-Smirnov distributions of total Al, Mg, and Fe ratio in the smectites in samples from continental rise sites BC495 (green solid line) and PC494 (MIS 2–4: red solid line) and PC494 and U1533 (MIS 5e: black solid line) in comparison to those from potential source areas on the Amundsen Sea shelf and slope (BC480: pink dotted line; BC36: brown dotted line; BC488: gray dotted line; BC27: yellow dotted line) and in the sub-Antarctic South Pacific basin (BC502: blue dotted line). (For interpretation of the references to colour in this figure legend, the reader is referred to the web version of this article.)

Hillenbrand et al., 2009b; Horrocks, 2018; Uenzelmann-Neben and Gohl, 2012) (Fig. 6). As for other parts of the West Antarctic margin, meltwater plumes may also have contributed to the deposition on the continental rise during times of maximum ice-sheet extent (Lucchi and Rebesco, 2007; Pudsey, 2000). This proposed depositional model is consistent with the previously reported increase of kaolinite in the glacial sediments on the Amundsen Sea rise (Hillenbrand et al., 2002; Hillenbrand et al., 2009b; Horrocks, 2018) and the dominance of Al-rich and Mg-poor smectites in the MIS 2-4 sediments at site PC494 reported here. The Al-Fe-Mg composition of smectites deposited on the continental rise during the last glacial period generally matches that of smectites characterizing the modern-late Holocene sediments on the continental shelf (BC488, BC480, BC27, and BC36). Conversely, there is no evidence for the contribution of any Mg-rich smectites from the sub-Antarctic South Pacific basin to the sediment deposition on the rise during glacials (Fig. 4), suggesting an only weak advection of deep and bottom waters, including CDW, towards the West Antarctic margin.

At the beginning of an interglacial period, the sedimentary processes on the Amundsen Sea continental rise were mainly controlled by the retreat of the WAIS from the outer shelf. The grounding line of the WAIS started to retreat towards today's coastline of the Amundsen Sea embayment (cf. Larter et al., 2014), and the long-lasting annual sea ice cover over the continental slope and rise gave way to longer openmarine conditions throughout the year (Bostock et al., 2013). With

progressive grounded ice retreat the smectite contents on the rise, like in the modern-late Holocene sediments at site BC495 and the MIS 5e sediments at site PC494, increased in response to reduced offshore supply of kaolinite enriched detritus (Hillenbrand et al., 2009b; Horrocks, 2018). During interglacial periods terrigenous detritus was transported from West Antarctica to the continental rise mainly as iceberg rafted debris (IRD), which comprises material of all grain sizes, with the icebergs drifting within surface currents associated with the Antarctic Coastal Current and the ACC (Lucchi et al., 2002). This is also documented by the predominance of Al rich smectites with intermediate Fe contents in the interglacial sediment samples from cores BC495, PC494 and U1533 (Fig. 4). In contrast, aeolian supply of detritus to the West Antarctic continental rise was negligible during interglacial periods because the terrigenous component of the interglacial sediments is dominated by detritus derived from West Antarctica rather than dust derived from South America or Australia (e.g., Wengler et al., 2019).

In addition to the Antarctica-derived detritus, the presence of Mgenriched smectites in the interglacial sediments at rise sites BC495, PC494 and U1533 indicates supply of fine-grained particles from the sub-Antarctic South Pacific basin (Fig. 4). These Mg-rich smectites were current-transported to the continental rise within deep and bottom waters, such as CDW, that probably flowed eastward within the ACC before being advected southward towards the Antarctic continental margin (Fig. 1). Both sediment core data from the Amundsen Sea shelf

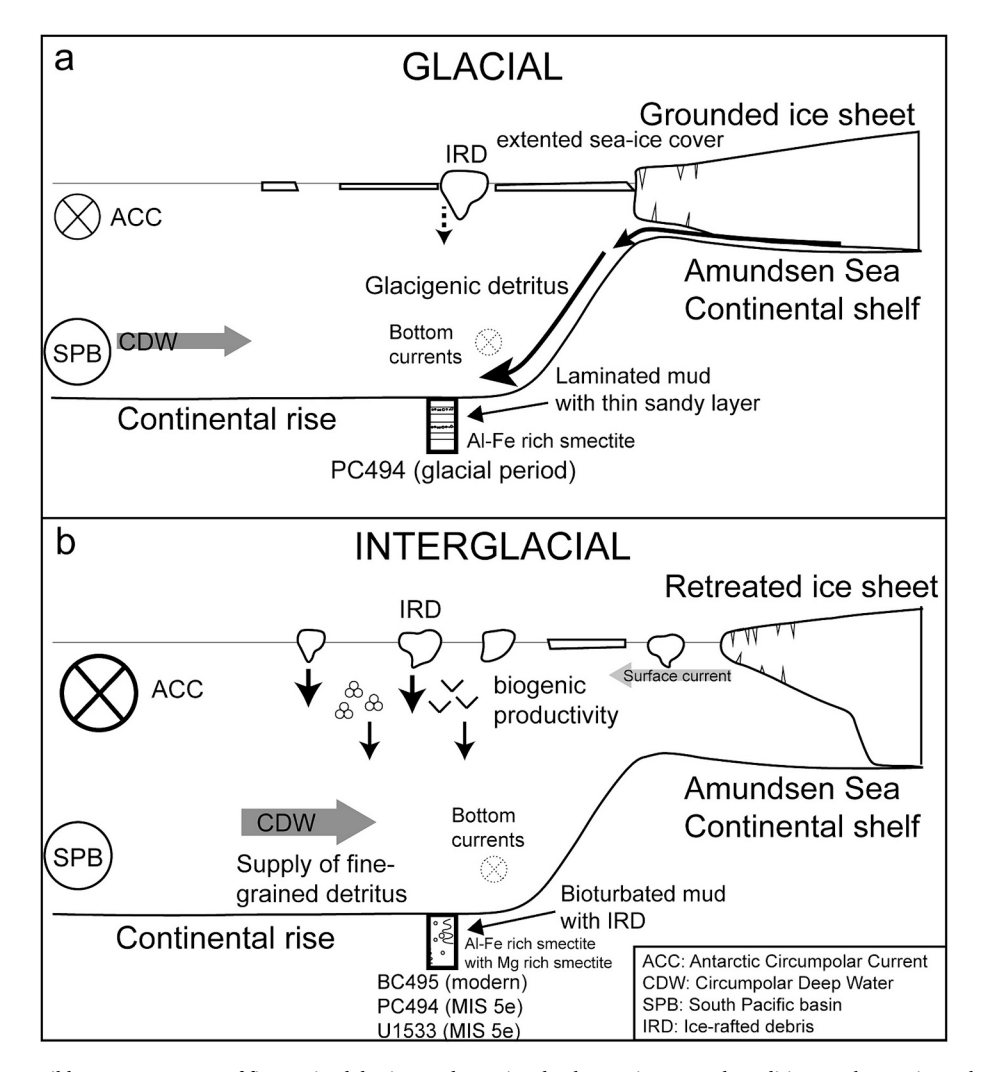


Fig. 6. Cartoon showing possible transport routes of fine-grained detritus and associated paleo-environmental conditions at the continental margin of the Amundsen Sea throughout a late Quaternary glacial-interglacial cycle. (a) During glacial periods, the main source of sediment deposited on the continental rise is supply of glacigenic detritus, including Al-rich smectites, from the Amundsen Sea shelf transported by gravitational down-slope processes, including turbidity currents, and meltwater plumes. (b) During interglacials, the terrigenous components deposited on the rise consist of detritus, including Al-rich smectites delivered by iceberg rafting from the Amundsen Sea coast, but also of fine-grained detritus, including Mg rich smectites, originating from the sub-Antarctic South Pacific basin and advected by deep and bottom waters, such as CDW, towards the Amundsen Sea continental margin. Eastward ACC flow was stronger during interglacial periods than during glacial times (Toyos et al., 2020).

and ice-sheet models had previously indicated that intensified CDW advection towards the West Antarctic margin played a crucial role in forcing WAIS retreat from the outer shelf during past deglaciations (Hillenbrand et al., 2017; Pollard and DeConto, 2009).

### 5. Conclusions

Glacial-interglacial provenance changes of sediments from the Amundsen Sea continental rise were investigated by comparing the elemental composition of smectite clay minerals with those of potential sources areas. Al—Fe rich smectite (dioctahedral smectite dominant) in glacial sediment are mainly originated with detritus derived from weathering products of igneous rock or sedimentary material. Conversely, with progressive grounded ice retreat, the presence of Mgrich smectite (montmorillonites and/or some trioctahedral smectites) could be supplied by the current-transportation, such as CDW, that advected southward towards the Antarctic continental margin. The observed glacial-interglacial changes in smectite composition can be explained by varying contributions from smectite sources located under the Amundsen Sea drainage sector of the WAIS and on the Amundsen Sea continental shelf on one hand and the sub-Antarctic South Pacific

basin on the other hand. The new results help to develop and refine a sediment transport and depositional model for the Amundsen Sea continental margin throughout late Quaternary glacial-interglacial cycles in relation to paleo-environmental changes, especially past WAIS dynamics.

### CRediT authorship contribution statement

Young Kyu Park: Writing – original draft, Methodology, Investigation, Data curation. Claus-Dieter Hillenbrand: Writing – review & editing, Data curation. Werner Ehrmann: Writing – review & editing, Methodology. Hanbeom Park: Methodology. Julia S. Wellner: Methodology. Jennifer R. Horrocks: Methodology. Jinwook Kim: Writing – review & editing, Supervision, Resources, Methodology, Investigation, Data curation, Conceptualization.

### Declaration of competing interest

The authors declare that they have no known competing financial interests or personal relationships that could have appeared to influence the work reported in this paper.

#### Data availability

Data will be made available on request.

### Acknowledgement

The present research was supported by the National Research Foundation of Korea (NRF) grant funded by the Korea government (MSIP) (NRF-2021R1A2C1003581) and Korea Polar Research Institute (KOPRI) grant funded by the Ministry of Oceans and Fisheries (KOPRI PE22090) to JWK. C.-D.H. was funded by NERC grant NE/S006664/1 and NERC UK-IODP grant NE/T010975/1. J.S.W. was supported by NSFPLR award no. 1738942. This work used samples and data provided by the International Ocean Discovery Program (IODP). We thank the captains, crews, technical support staff and scientific parties of expeditions JR179 with RRS James Clark Ross, NBP2002 with RV/IB Nathaniel B. Palmer and IODP Expedition 379 with RV JOIDES Resolution.

### Appendix A. Supplementary data

Supplementary data to this article can be found online at https://doi.org/10.1016/j.chemgeo.2024.122116.

#### References

- Aoudjit, H., Robert, M., Elsass, F., Curmi, P., 1995. Detailed study of smectite genesis in granitic saprolites by analytical electron microsopy. Clay Miner. 30 (2), 135–147.
- Biscaye, P.E., 1964. Distinction between kaolinite and chlorite in recent sediments by X-ray diffraction. Am. Mineral. 49 (9–10), 1281–1289.
- Biscaye, P.E., 1965. Mineralogy and sedimentation of recent deep-sea clay in the Atlantic Ocean and adjacent seas and oceans. Geol. Soc. Am. Bull. 76 (7), 803–832.
- Bostock, H.C., Barrows, T.T., Carter, L., Chase, Z., Cortese, G., Dunbar, G.B., Ellwood, M., Hayward, B., Howard, W., Neil, H., 2013. A review of the Australian–New Zealand sector of the Southern Ocean over the last 30 ka (Aus-INTIMATE project). Quat. Sci. Rev. 74, 35–57.
- Chamley, H., 1989. Clay formation through weathering. In: Chamley, H. (Ed.), Clay Sedimentology. Springer, Berlin, Heidelberg, pp. 21–50.
- Chamley, H., 1994. Clay mineral diagenesis. Nato Asi Ser. C Math. Phys. Sci. 453, 161.
  Chang, H.K., Mackenzie, F.T., Schoonmaker, J., 1986. Comparisons between the diagenesis of dioctahedral and trioctahedral smectite, Brazilian offshore basins. Clay Clay Miner. 34, 407–423.
- Christidis, G., Chryssikos, G., Derkowski, A., Dohrmann, R., Eberl, D., Joussein, E., Kaufhold, S., 2023. Methods for determination of the layer charge of smectites: a critical assessment of existing approaches. Clay Clay Miner. 71, 1–29.
- Clark, R., Wellner, J., Hillenbrand, C., Totten, R., Smith, J., Simkins, L., Larter, R., Hogan, K., Graha, A., Nitsche, F., 2024. Synchronous retreat of Thwaites and Pine Island glaciers in response to external forcings in the presatellite era. P. Natl. Acad. Sci. 121 (11).
- Cliff, G., Lorimer, G.W., 1975. The quantitative analysis of thin specimens. J. Microsc.  $103\ (2),\ 203-207.$
- Conconi, R., Ventruti, G., Nieto, F., Capitani, G., 2023. TEM-EDS microanalysis: Comparison among the standardless, Cliff & Lorimer and absorption correction quantification methods. Ultramicroscopy 254, 113845.
- Cook, C.P., Van De Flierdt, T., Williams, T., Hemming, S.R., Iwai, M., Kobayashi, M., Jimenez-Espejo, F.J., Escutia, C., González, J.J., Khim, B.-K., 2013. Dynamic behaviour of the East Antarctic ice sheet during Pliocene warmth. Nat. Geosci. 6 (9), 765–769.
- de Vries, M.V.W., Bingham, R.G., Hein, A.S., 2018. A new volcanic province: an inventory of subglacial volcanoes in West Antarctica. Geol. Soc. Lond. Spec. Publ. 461 (1), 231–248.
- Deconinck, J., Chamley, H., 1995. Diversity of smectite origins in late cretaceous sediments: example of chalks from northern France. Clay Miner. 30 (4), 365–379.
- DeConto, R.M., Pollard, D., 2016. Contribution of Antarctica to past and future sea-level rise. Nature 531 (7596), 591–597.
- Dorschel, B., Hehemann, L., Viquerat, S., Warnke, F., Dreutter, S., Tenberge, Y.S., Accettella, D., An, L., Barrios, F., Bazhenova, E., 2022. The international bathymetric chart of the southern ocean version 2. Scientific Data 9 (1), 275.
- Dowdeswell, J.A., Evans, J., O'Cofaigh, C., Anderson, J.B., 2006. Morphology and sedimentary processes on the continental slope off Pine Island Bay, Amundsen Sea, West Antarctica. Geol. Soc. Am. Bull. 118 (5–6), 606–619.
- Drief, A., Nieto, F., 2000. Chemical composition of smectites formed in clastic sediments. Implications for the smectite-illite transformation. Clay Miner. 35 (4), 665–678.
- Drits, V., Sakharov, B., 1976. X-ray structural analysis of mixed-layer minerals. Trans. Acad. Sci. 295, 1–252.
- Dutton, A., Carlson, A.E., Long, A.J., Milne, G.A., Clark, P.U., DeConto, R., Horton, B.P., Rahmstorf, S., Raymo, M.E., 2015. Sea-level rise due to polar ice-sheet mass loss during past warm periods. Science 349 (6244).

- Ehrmann, W., Hillenbrand, C.D., Smith, J.A., Graham, A.G.C., Kuhn, G., Larter, R.D., 2011. Provenance changes between recent and glacial-time sediments in the Amundsen Sea embayment, West Antarctica: clay mineral assemblage evidence. Antarct. Sci. 23 (5), 471–486.
- Elert, K., Azañón, J.M., Nieto, F., 2018. Smectite formation upon lime stabilization of expansive marls. Appl. Clay Sci. 158, 29–36.
- Escutia, C., Bárcena, M., Lucchi, R., Romero, O., Ballegeer, A., Gonzalez, J., Harwood, D., 2009. Circum-Antarctic warming events between 4 and 3.5 Ma recorded in marine sediments from the Prydz Bay (ODP Leg 188) and the Antarctic Peninsula (ODP Leg 178) margins. Glob. Planet. Chang. 69 (3), 170–184.
- Esper, O., Gersonde, R., 2014. New tools for the reconstruction of Pleistocene Antarctic Sea ice. Palaeogeogr. Palaeoclimatol. Palaeoecol. 399, 260–283.
- García-Romero, E., Vegas, J., Baldonedo, J., Marfil, R., 2005. Clay minerals as alteration products in basaltic volcaniclastic deposits of La Palma (Canary Islands, Spain). Sediment. Geol. 174 (3–4), 237–253.
- García-Romero, E., Lorenzo, A., García-Vicente, A., Morales, J., García-Rivas, J., Suárez, M., 2021. On the structural formula of smectites: a review and new data on the influence of exchangeable cations. J. Appl. Crystallogr. 54 (1), 251–262.
- Gohl, K., Uenzelmann-Neben, G., Larter, R.D., Hillenbrand, C.-D., Hochmuth, K., Kalberg, T., Weigelt, E., Davy, B., Kuhn, G., Nitsche, F.O., 2013. Seismic stratigraphic record of the Amundsen Sea Embayment shelf from pre-glacial to recent times: evidence for a dynamic West Antarctic ice sheet. Mar. Geol. 344, 115–131.
- Gohl, K., Freudenthal, T., Hillenbrand, C.D., Klages, J., Larter, R., Bickert, T., Bohaty, S., Ehrmann, W., Esper, O., Frederichs, T., 2017. MeBo70 seabed drilling on a polar continental shelf: Operational report and lessons from drilling in the Amundsen Sea Embayment of West Antarctica. Geochem. Geophys. Geosyst. 18 (11), 4235–4250.
- Gohl, K., Wellner, J., Klaus, A., 2021. Amundsen Sea West Antarctic Ice Sheet history. Proceedings of the International Ocean Discovery Program, 379.
- Hillenbrand, C.D., Ehrmann, W., 2001. Distribution of clay minerals in drift sediments on the continental rise west of the Antarctic Peninsula, ODP Leg 178, Sites 1095 and 1096. In: Barker, P.F., Camerlenghi, A., Acton, G.D., Ramsay, A.T.S. (Eds.), Proc. ODP, Sci. Results, 178 [Online]. Available from World Wide Web: http://www-odp. tamu.edu/publications/178 SR/VOLUME/CHAPTERS/SR178 08.PDF.
- Hillenbrand, C.D., Ehrmann, W., 2005. Late Neogene to Quaternary environmental changes in the Antarctic Peninsula region: evidence from drift sediments. Glob. Planet. Chang. 45 (1–3), 165–191.
- Hillenbrand, C.D., Fütterer, D.K., Grobe, H., Frederichs, T., 2002. No evidence for a Pleistocene collapse of the West Antarctic Ice Sheet from continental margin sediments recovered in the Amundsen Sea. Geo-Mar. Lett. 22, 51–59.
- Hillenbrand, C.D., Grobe, H., Diekmann, B., Kuhn, G., Futterer, D.K., 2003. Distribution of clay minerals and proxies for productivity in surface sediments of the Bellingshausen and Amundsen seas (West Antarctica) - Relation to modern environmental conditions. Mar. Geol. 193 (3-4), 253-271.
- Hillenbrand, C.D., Ehrmann, W., Larter, R.D., Benetti, S., Dowdeswell, J.A., Cofaigh, C. O., Graham, A.G.C., Grobe, H., 2009a. Clay mineral provenance of sediments in the southern Bellingshausen Sea reveals drainage changes of the West Antarctic Ice Sheet during the late Quaternary. Mar. Geol. 265 (1–2), 1–18.
- Hillenbrand, C.D., Kuhn, G., Frederichs, T., 2009b. Record of a Mid-Pleistocene depositional anomaly in West Antarctic continental margin sediments: an indicator for ice-sheet collapse? Quat. Sci. Rev. 28 (13–14), 1147–1159.
- Hillenbrand, C.D., Larter, R.D., Dowdeswell, J.A., Ehrmann, W., Cofaigh, C.O., Benetti, S., Graham, A.G.C., Grobe, H., 2010. The sedimentary legacy of a palaeo-ice stream on the shelf of the southern Bellingshausen Sea: Clues to West Antarctic glacial history during the late Quaternary. Quat. Sci. Rev. 29 (19–20), 2741–2763.
- Hillenbrand, C.D., Kuhn, G., Smith, J.A., Gohl, K., Graham, A.G., Larter, R.D., Klages, J. P., Downey, R., Moreton, S.G., Forwick, M., 2013. Grounding-line retreat of the West Antarctic ice sheet from inner Pine island Bay. Geology 41 (1), 35–38.
- Hillenbrand, C.D., Smith, J.A., Hodell, D.A., Greaves, M., Poole, C.R., Kender, S., Williams, M., Andersen, T.J., Jernas, P.E., Elderfield, H., Klages, J.P., Roberts, S.J., Gohl, K., Larter, R.D., Kuhn, G., 2017. West Antarctic Ice Sheet retreat driven by Holocene warm water incursions. Nature 547 (7661), 43–48.
- Hillenbrand, C.D., Crowhurst, S., Williams, M., Hodell, D., McCave, I., Ehrmann, W., Xuan, C., Piotrowski, A., Hernández-Molina, F., Graham, A., 2021. New insights from multi-proxy data from the West Antarctic continental rise: Implications for dating and interpreting late Quaternary palaeoenvironmental records. Quat. Sci. Rev. 257, 106842.
- Hillier, S., 1995. Erosion, sedimentation and sedimentary origin of clays. In: Velde, B. (Ed.), Origin and Mineralogy of Clays: Clays and the Environment. Springer, Berlin, Heidelberg, pp. 162–219.
- Hollister, C.D., Worstell, P., 1976. Initial reports of the deep sea drilling project. In: Covering Leg 35 of the Cruises of the Drilling Vessel "Glomar Challenger", Callao, Peru, to Ushuaia, Argentina, February-March 1974, vol. 35. U.S. Government Printing Office.
- Horrocks, J., 2018. The Formation and Late Quaternary Palaeoenvironmental History of Sediment Mounds in the Amundsen Sea, West Antarctica. PhD Thesis. Department of Geography, Durham University.
- Jackson, M.L., 1969. Soil Chemical Analysis: Advanced Course, Edition 2. Madison, Wisconsin.
- Jacobs, S., Jenkins, A., Hellmer, H., Giulivi, C., Nitsche, F., Huber, B., Guerrero, R., 2012. The Amundsen Sea and the Antarctic ice sheet. Oceanography 25 (3), 154–163.
- Jenkins, A., Dutrieux, P., Jacobs, S., Steig, E.J., Gudmundsson, G.H., Smith, J., Heywood, K.J., 2016. Decadal Ocean forcing and Antarctic ice sheet response: Lessons from the Amundsen Sea. Oceanography 29 (4), 106–117.
- Jeong, G.Y., Yoon, H.I., Lee, S.Y., 2004. Chemistry and microstructures of clay particles in smectite-rich shelf sediments, South Shetland Islands, Antarctica. Mar. Geol. 209 (1–4), 19–30.

Y.K. Park et al. Chemical Geology 657 (2024) 122116

Jung, J., Yoo, K.C., Lee, K.H., Park, Y.K., Lee, J.I., Kim, J., 2019. Clay Mineralogical Characteristics of Sediments Deposited during the late Quaternary in the Larsen Ice Shelf B Embayment, Antarctica. Minerals 9 (3), 153.

- Kim, J.W., Peacor, D.R., Tessier, D., Elsass, F., 1995. A Technique for Maintaining Texture and Permanent expansion of Smectite Interlayers for Tem Observations. Clay Clay Miner. 43 (1), 51–57.
- Kim, J., Dong, H., Yang, K., Park, H., Elliott, W.C., Spivack, A., Koo, T.-H., Kim, G., Morono, Y., Henkel, S., 2019. Naturally occurring, microbially induced smectite-toillite reaction. Geology 47 (6), 535–539.
- Kirshner, A.E., Anderson, J.B., Jakobsson, M., O'Regan, M., Majewski, W., Nitsche, F.O., 2012. Post-LGM deglaciation in Pine island Bay, West Antarctica. Quat. Sci. Rev. 38, 11–26.
- Klages, J.P., Salzmann, U., Bickert, T., Hillenbrand, C.-D., Gohl, K., Kuhn, G., Bohaty, S. M., Titschack, J., Müller, J., Frederichs, T., 2020. Temperate rainforests near the South Pole during peak cretaceous warmth. Nature 580 (7801), 81–86.
- Konfirst, M.A., Scherer, R.P., Hillenbrand, C.D., Kuhn, G., 2012. A marine diatom record from the Amundsen - Sea Insights into oceanographic and climatic response to the Mid-Pleistocene transition in the West Antarctic sector of the Southern Ocean. Mar. Micropaleontol. 92-93. 40-51.
- Larter, R.D., Anderson, J.B., Graham, A.G.C., Gohl, K., Hillenbrand, C.D., Jakobsson, M., Johnson, J.S., Kuhn, G., Nitsche, F.O., Smith, J.A., Witus, A.E., Bentley, M.J., Dowdeswell, J.A., Ehrmann, W., Klages, J.P., Lindow, J., Cofaigh, C.O., Spiegel, C., 2014. Reconstruction of changes in the Amundsen Sea and Bellingshausen Sea sector of the West Antarctic Ice Sheet since the last Glacial Maximum. Quat. Sci. Rev. 100, 55-86
- Lau, S.C., Wilson, N.G., Golledge, N.R., Naish, T.R., Watts, P.C., Silva, C.N., Cooke, I.R., Allcock, A.L., Mark, F.C., Linse, K., 2024. Genomic evidence for West Antarctic Ice Sheet collapse during the last Interglacial Period. bioRxiv. https://doi.org/10.1101/ 2023.01.29.525778.
- LeMasurier, W., 2002. Architecture and evolution of hydrovolcanic deltas in Marie Byrd Land, Antarctica. In: Smellie, J.L. (Ed.), Volcano–Ice Interaction on Earth and Mars. Geological Society of London Special Publications, London, pp. 115–148.
- LeMasurier, W., 2013. Shield volcanoes of Marie Byrd Land, West Antarctic rift: oceanic island similarities, continental signature, and tectonic controls. Bull. Volcanol. 75,
- Licht, K.J., Hemming, S.R., 2017. Analysis of Antarctic glacigenic sediment provenance through geochemical and petrologic applications. Quat. Sci. Rev. 164, 1–24.
- Lucchi, R.G., Rebesco, M., 2007. Glacial contourites on the Antarctic Peninsula margin: insight for palaeoenvironmental and palaeoclimatic conditions. Geol. Soc. Lond. Spec. Publ. 276 (1), 111–127.
- Lucchi, R.G., Rebesco, M., Camerlenghi, A., Busetti, M., Tomadin, L., Villa, G., Persico, D., Morigi, C., Bonci, M.C., Giorgetti, G., 2002. Mid-late Pleistocene glacimarine sedimentary processes of a high-latitude, deep-sea sediment drift (Antarctic Peninsula Pacific margin). Mar. Geol. 189 (3–4), 343–370.
- Marshall, C., 1935. Layer lattices and the base-exchange clays. Zeitschrift für Kristallographie-Crystalline Materials 91 (1–6), 433–449.
- McCarty, D.K., Sakharov, B.A., Drits, V.A., 2009. New insights into smectite illitization: A zoned K-bentonite revisited. Am. Mineral. 94 (11–12), 1653–1671.
- McKinley, J., Worden, R., Ruffell, A., 1999. Smectite in sandstones: A review of the controls on occurrence and behaviour during diagenesis. In: Worden, Richard H., S.
   M. (Eds.), Clay Mineral Cements in Sandstones. Blackwell Publishing, International Association of Sedimentologists, pp. 109–128.
- Mcmurtry, G.M., Yeh, H.W., 1981. Hydrothermal Clay Mineral Formation of East Pacific rise and Bauer Basin Sediments. Chem. Geol. 32 (3–4), 189–205.
- Moore, D.M., Reynolds Jr., R.C., 1989. X-Ray Diffraction and the Identification and Analysis of Clay Minerals. Oxford University Press (OUP).
- Nieto, F., Ortega-Huertas, M., Peacor, D., Arostegui, J., 1996. Evolution of illite/smectite from early diagenesis through incipient metamorphism in sediments of the Basque-Cantabrian Basin. Clay Clay Miner. 44, 304–323.
- Pandarinath, K., 2009. Clay minerals in SW Indian continental shelf sediment cores as indicators of provenance and palaeomonsoonal conditions: a statistical approach. Int. Geol. Rev. 51 (2), 145–165.
- Park, Y.K., Lee, J.I., Jung, J., Hillenbrand, C.D., Yoo, K.C., Kim, J., 2019. Elemental compositions of smectites reveal detailed sediment provenance changes during glacial and interglacial periods: the southern drake passage and Bellingshausen Sea, Antarctica. Minerals 9 (5), 322.
- Park, H., Yang, K., Koo, T.-H., Kang, I., Yamamoto, Y., Kim, J., 2024. Physico-chemical properties of illite in the organic matter (OM)-rich claystone of Nankai Trough

- contrast with coeval OM-poor claystone: IODP Expedition 348. Appl. Clay Sci. 250, 107267.
- Petschick, R., Kuhn, G., Gingele, F., 1996. Clay mineral distribution in surface sediments of the South Atlantic: sources, transport, and relation to oceanography. Mar. Geol. 130 (3–4), 203–229.
- Pollard, D., DeConto, R.M., 2009. Modelling West Antarctic ice sheet growth and collapse through the past five million years. Nature 458 (7236), 329–U89.
- Pritchard, H., Ligtenberg, S.R., Fricker, H.A., Vaughan, D.G., van den Broeke, M.R., Padman, L., 2012. Antarctic ice-sheet loss driven by basal melting of ice shelves. Nature 484 (7395), 502–505.
- Pudsey, C.J., 2000. Sedimentation on the continental rise west of the Antarctic Peninsula over the last three glacial cycles. Mar. Geol. 167 (3-4), 313-338.
- Righi, D., Meunier, A., 1995. Origin of clays by rock weathering and soil formation. In: Velde, B. (Ed.), Origin and Mineralogy of Clays: Clays and the Environment. Springer, Berlin, Heidelberg, pp. 43–161.
- Rignot, E., Mouginot, J., Scheuchl, B., Van Den Broeke, M., Van Wessem, M.J., Morlighem, M., 2019. Four decades of Antarctic Ice Sheet mass balance from 1979–2017. Proc. Natl. Acad. Sci. 116 (4), 1095–1103.
- Sánchez-Roa, C., Bauluz, B., Nieto, F., Abad, İ., Jimenéz-Millán, J., Faulkner, D., 2018. Micro-and nano-scale study of deformation induced mineral transformations in Mg-phyllosilicate-rich fault gouges from the Galera Fault Zone (Betic Cordillera, SE Spain). Am. Mineral. 103 (10), 1604–1621.
- Simões Pereira, P., van de Flierdt, T., Hemming, S.R., Hammond, S.J., Kuhn, G., Brachfeld, S., Doherty, C., Hillenbrand, C.D., 2018. Geochemical fingerprints of glacially eroded bedrock from West Antarctica: Detrital thermochronology, radiogenic isotope systematics and trace element geochemistry in late Holocene glacial-marine sediments. Earth Sci. Rev. 182, 204–232.
- Simões Pereira, P., van de Flierdt, T., Hemming, S.R., Frederichs, T., Hammond, S.J., Brachfeld, S., Doherty, C., Kuhn, G., Smith, J.A., Klages, J.P., Hillenbrand, C.D., 2020. The geochemical and mineralogical fingerprint of West Antarctica's weak underbelly. Pine Island and Thwaites glaciers. Chem. Geol. 550, 119649.
- Smith, B., Fricker, H.A., Gardner, A.S., Medley, B., Nilsson, J., Paolo, F.S., Holschuh, N., Adusumilli, S., Brunt, K., Csatho, B., 2020. Pervasive ice sheet mass loss reflects competing ocean and atmosphere processes. Science 368 (6496), 1239–1242.
- Stuart, A., Ord, K., 1999. S. Arnold Kendall's Advanced Theory of Statistics. In: Classical Inference and the Linear Model, vol. 2A. Arnold Publishers.
- Totten, R.L., Majewski, W., Anderson, J.B., Yokoyama, Y., Fernandez, R., Jakobsson, M., 2017. Oceanographic influences on the stability of the Cosgrove Ice Shelf, Antarctica. The Holocene 27 (11), 1645–1658.
- Toyos, M.H., Lamy, F., Lange, C.B., Lembke-Jene, L., Saavedra-Pellitero, M., Esper, O., Arz, H.W., 2020. Antarctic Circumpolar Current Dynamics at the Pacific Entrance to the Drake Passage over the past 1.3 Million Years. Paleoceanogr. Paleoclimatol. 35 (7) e2019PA003773.
- Uenzelmann-Neben, G., Gohl, K., 2012. Amundsen Sea sediment drifts: archives of modifications in oceanographic and climatic conditions. Mar. Geol. 299, 51–62.
- Vaughan, D.G., 2008. West Antarctic Ice Sheet collapse the fall and rise of a paradigm. Clim. Chang. 91 (1–2), 65–79.
- Velde, B., 1995. Composition and mineralogy of clay minerals. In: Velde, B. (Ed.), Origin and Mineralogy of Clays: Clays and the Environment. Springer, Berlin, Heidelberg, pp. 8–42.
- Weaver, C., Pollard, L., 1973. Developments in sedimentology. In: The Chemistry of Clay Minerals, vol. 15. Elsevier Sci, New York.
- Wengler, M., Lamy, F., Struve, T., Borunda, A., Böning, P., Geibert, W., Kuhn, G., Pahnke, K., Roberts, J., Tiedemann, R., 2019. A geochemical approach to reconstruct modern dust fluxes and sources to the South Pacific. Geochim. Cosmochim. Acta 264, 205–223.
- Williams, T., van de Flierdt, T., Hemming, S.R., Chung, E., Roy, M., Goldstein, S.L., 2010. Evidence for iceberg armadas from East Antarctica in the Southern Ocean during the late Miocene and early Pliocene. Earth Planet. Sci. Lett. 290 (3–4), 351–361.
- Wilson, D.J., Bertram, R.A., Needham, E.F., van de Flierdt, T., Welsh, K.J., McKay, R.M., Mazumder, A., Riesselman, C.R., Jimenez-Espejo, F.J., Escutia, C., 2018. Ice loss from the East Antarctic Ice Sheet during late Pleistocene interglacials. Nature 561 (7723), 383–386.
- Yang, K., Kim, J.W., Kogure, T., Dong, H.L., Baik, H., Hoppie, B., Harris, R., 2016. Smectite, illite, and early diagenesis in South Pacific Gyre subseafloor sediment. Appl. Clay Sci. 134, 34–43.